Freie Universität Berlin
Department of Physics
Arnimallee 14
14195 Berlin

WS 2011/12

Advanced Lab Course for Master Students
Report

Ma3 - Pulsed Nuclear Magnetic Resonance Spectroscopy

Stefanie Kreft
kreft@physik.fu-berlin.de

Samuel Sanchez Viveros
sanchez@physik.fu-berlin.de

December 19, 2011

Tutor: Ch. Meier

Contents

1 Theoretical Background **1**
- 1.1 Nuclear Spin . . . 1
  - 1.1.1 Magnetic Moment and Magnetization . . . 1
- 1.2 Spin Dynamics . . . 2
  - 1.2.1 Spin-Spin-Relaxation . . . 3
  - 1.2.2 Spin-Lattice-Relaxation . . . 4
  - 1.2.3 Bloch-Equations . . . 4
- 1.3 Experimental Methods . . . 5
  - 1.3.1 Measurement of T_2^* via Free Induction Decay . . . 5
  - 1.3.2 Measurement of T_1 via Inversion Recovery . . . 5
  - 1.3.3 Measurement of T_2 . . . 5

2 Experimental Setup and Procedure **7**
- 2.1 Experimental Setup . . . 7
- 2.2 Experimental Procedure . . . 7

3 Experimental Results and Analysis **9**
- 3.1 Calibration of Pulse Duration . . . 9
- 3.2 Inhomogeneity of the External Magnetic Field . . . 9
- 3.3 Longitudinal Relaxation Time T_1 . . . 12
- 3.4 Transversal Relaxation Time T_2 . . . 13
  - 3.4.1 Measurement via Spin-Echo-Methode . . . 13
  - 3.4.2 Measurement via Carr-Purcell-Methode . . . 13
  - 3.4.3 Measurement via Meiboom-Gill-Methode . . . 16
- 3.5 Influence of Concentration of $CuSO_4$ . . . 18

4 Conclusion **19**

1 Theoretical Background

Nuclear magnetic resonance was first observed in 1945 and results were first published 1946 by Edward Purcell and Felix Bloch simultaneously. They measured the response of a magnetic nuclei to continuous radio frequencies. In 1960, Erwin Hahn applied short pulses of magnetic fields in the range of radio frequencies to a probe of magnetic nuclei and thereby established the basis of pulsed nuclear magnetic resonance (PNMR) research. This provides a effective technique to determine local surrounding fields of nuclei inside probes via measuring relaxation times of spins. I.a. using PNMR different states of atoms in complex molecules like proteins can be investigated which give insights into their structure and behavior. Also, Magnetic resonance imaging is an vitally important tool used in Medical imaging which uses PNMR.

1.1 Nuclear Spin

Neutrons and Protons are fermionic particles i.e. with spin $\frac{1}{2}\hbar$. Nuclei as particles composed of fermions can thus have a non-vanishing or vanishing total spin and therefore be a bosonic or fermionic particle. For nuclei composed of an even number of neutrons and protons (so called gg-nuclei) the spin vanishes in the ground state, because due to Pauli's exclusion principle all spins are pairwise antiparallel aligned. If either number of nucleons is odd (i.e. gu-, ug,- or uu-nuclei) the nucleus can posses a total nuclear spin $\hbar\vec{I} \neq 0$.

1.1.1 Magnetic Moment and Magnetization

The nuclear is connected to the magnetic moment of the core $\vec{\mu}$ via

$$\vec{\mu} = \gamma\hbar\vec{I} = \frac{e\hbar}{2m} g\vec{I}\,, \tag{1.1.1}$$

where γ denotes the gyromagnetic ratio, e the elementary charge, m the mass of either proton or neutron (which are in good approximation equal) and g is the g-factor. Measurements of the g-factor for protons and neutrons yield

$$g_p = 5.585\,694\,713(46) \qquad g_n = -3.826\,085\,45(90)\,, \text{ [1]} \tag{1.1.2}$$

which can be explained by the inner structure of the nucleons. Due to interaction of the spins with each other the total magnetic moment of a composite particle is not equal to the g-factor weighted sum over all spins. However, γ can be understood as empiric parameter which can be easily fixed via measurements using (1.1.1).
Projecting the total nuclear spin $\vec{I}$ onto the core-internal z-axis (w.l.o.g.) and considering the quantum mechanical properties of spin yields the quantized magnetic quantum number m_z as eigenvalue of $\hat{I}_z$ with the spectrum $m_z = \{0, \pm 1, \ldots, \pm I\}$. If a magnetic field is absent m_z labels the degeneracy of a state with total spin $\vec{I}$. In an ensemble of free nuclei the z-axes of all the cores are randomly uniformly distributed leading to a vanishing net magnetization

$\vec{M} = \sum_i \mu_i$. By applying an external magnetic field a preferred magnetization orientation is created by defining a global z-axis pointing in the direction of the magnetic field $\vec{e}_B$. Thus, a total net magnetization is given by the projection of all single core magnetic moments onto the direction of the field

$$\vec{M} \cdot \vec{e}_B = \sum_i \gamma_i \hbar \, m_{z,i} \, . \tag{1.1.3}$$

Furthermore, if an external magnetic field is applied, the cores exhibit a Zeeman-splitting of the energy levels which is given by

$$\Delta E_{m,m+1} = \gamma \hbar B \, . \tag{1.1.4}$$

In thermal equilibrium the partition function of this multi-particle two-level system yield that the states follow a Boltzmann distribution with yield for the ratio of occupation number for the states α and β, which labels the spin states up and down,

$$\frac{N_\alpha}{N_\beta} = \exp\left\{ (m_{z,\alpha} - m_{z,\beta}) \, \frac{\gamma \hbar B}{3 k_B T} \right\} = \exp\left\{ -\frac{\Delta E_{\alpha,\beta}}{k_B T} \right\} \, . \tag{1.1.5}$$

In thermal equilibrium and in presence of a external magnetic field $\vec{B}_0$ this give rise to a finite net magnetization, which can be derived from (1.1.5) by normalizing with $N = N_\alpha + N_\beta$ and expanding in first order with respect to $k_B T \gg \Delta E$

$$\vec{M}_0 = \frac{n \gamma^2 \hbar^2 I(I+1)}{k_B T} \vec{B}_0 \, , \tag{1.1.6}$$

where $n = N/V$ is here the number of spins per unit volume. [2]

1.2 Spin Dynamics

Considering the dynamic case i.e. not in thermal equilibrium, the magnetic momenta are not aligned parallel to the external magnetic field. The external magnetic field causes a torque resulting in a precession of magnetic momenta with respect to the direction of the external field with the frequency

$$\omega_L = \gamma B_0 \, . \tag{1.2.1}$$

This so called Larmor frequency ω_L equals in magnitude the resonance frequency for dipolar transitions with selection rules $\Delta M = \pm 1$.
The equation of motion is given by

$$\dot{\vec{M}} = \gamma \vec{M} \times \vec{B}_0 \tag{1.2.2}$$

As already mentioned this describes a precession of the magnetic field around $\vec{B}_0$ with the Larmor frequency. If a magnetic field consisting of a space and time homogenous magnetic

field $\vec{B}_0$ and and space homogenous and in time oscillating field $\vec{B}_1(t)$ with frequency ω_L and perpendicular to $\vec{B}_0$ is applied, the equation of motion becomes

$$\begin{aligned}\dot{\vec{M}} &= \gamma\vec{M} \times \left(\vec{B}_0 + \vec{B}_1(t)\right) \\ \dot{\vec{M}} - \vec{M} \times \gamma\vec{B}_0 &= \gamma\vec{M} \times \vec{B}_1(t) \\ \dot{\vec{M}} - \vec{\omega}_L \times \vec{M} &= \gamma\vec{M} \times \vec{B}_1(t)\,. \end{aligned} \tag{1.2.3}$$

The left hand side of this equation can be identified as time derivative in a rotating reference frame and thus can be rewritten as

$$\left(\partial_t \vec{M}\right)_{rot} = \gamma\vec{M} \times \vec{B}_1(t)\,, \tag{1.2.4}$$

where $\vec{B}_1(t)$ is now stationary and causes the magnetization to precess around it. This can be described by an angular velocity and thus by an equation of motion for the angle θ at which the magnetization has rotated around $\vec{B}_1$. Assuming, that as long as $\vec{B}_1$ is turned on it is constant and neglecting any rise and fall times during the switching process, the angle θ is given by

$$\omega = \dot{\theta} = \gamma B_1 \Rightarrow \theta = \gamma B_1 \mathfrak{t}\,, \tag{1.2.5}$$

where $\mathfrak{t}$ is the pulse duration. Thus, by choosing an appropriate pulse length of the magnetic field $\vec{B}_1$ the magnetization can be rotated by an arbitrary angle, especially $\frac{\pi}{2}$ and π, thus inverting the magnetization or turning it into the xy-plane.

1.2.1 Spin-Spin-Relaxation

In presence of a magnetic field chosen to point into the z-direction only the z component M_z of the total net magnetic momentum $\vec{M}$ corresponds to a Zeeman energy and therefore a change of M_x and M_y does not alter the total energy of the system. In the dynamic, non-equilibrium state, the system seeks to restore thermal equilibrium, i.e. a parallel alignment of $\vec{M}$ to the external magnetic field. Thus, the components M_x and M_y will decay through different processes without energy transfers to the surroundings [2]. This is called Spin-Spin-Relaxation.
The rate of change of this two components is given by

$$\dot{M}_{x,y} = -\frac{M_{x,y}}{T_2}\,. \tag{1.2.6}$$

The solution of this differential equation yields an exponential decay of the two components, which is given by

$$M_{x,y}(t) = M_{x,y}(t=0)e^{-\frac{t}{T_2}}\,, \tag{1.2.7}$$

where T_2 is called transversal relaxation time.

1.2.2 Spin-Lattice-Relaxation

The M_z component of the total spin would undergo the same relaxation process as the transversal components if inverted. However, to allow any decay the spin system must transfer energy to the surroundings, due to the Zeeman effect. This is called spin-lattice-relaxation, where the term lattice denotes a system coupled to the spin system which absorbs the energy set free by decay. In solids, this is indeed the lattice but in general it can be any degree of freedom. Furthermore, M_z does not vanish in thermal equilibrium but approaches the steady state net magnetization $\vec{M}_0 = M_0 \hat{e_z}$ given by (1.1.6). Thus relaxation obeys the equation

$$\dot{M}_z = -\frac{M_z - M_0}{T_1} \tag{1.2.8}$$

Due to the fact, that the spin-lattice-relaxation requires energy transfers but is caused by the same perturbations as the spin-spin-relaxation, it is reasonable that the relaxation times fulfill

$$T_2 \leq T_1 \,. \tag{1.2.9}$$

One additional relaxation process of importance is caused by dephasing of the magnetic moments due to inhomogeneities of the static magnetic field $\vec{B}_0$. Applying a $\frac{\pi}{2}$-pulse changes the direction of the net magnetization $\vec{M}_0$ into the xy-plane. The net magnetization still precesses around $\vec{B}_0$ according to (1.2.2). However, due to the inhomogeneities of $\vec{B}_0$ the magnetic moments in the sample will dephase due to different precession frequencies and vanish after a characteristic time T_2^*. This effect is also present during both the other relaxation processes and thus

$$T_2^* \leq T_2 \leq T_1 \tag{1.2.10}$$

is reasonable.
To give an reasonable estimation of T_1 and T_2 a microscopic understanding and a description of the magnetic environment is required. In paramagnetic salts dissolved in water, the sample exhibits a strong spin-spin-interaction and large perturbations by the magnetic moments of unpaired electrons. A reasonable assumption for this sample is

$$T_1^{-1} = k_1 n \,, \tag{1.2.11}$$

where n is the concentration of the salt and k_1 a suitable constant, which can be determined by experiments.

1.2.3 Bloch-Equations

All effects mentioned earlier can be described by a set coupled differential equations for each component of $\vec{M}$. These are called Bloch-equations and are given by

$$\dot{M}_x = \gamma \left[M_y B_0 + M_z B_1 \sin(\omega t) \right] - \frac{M_x}{T_2} \tag{1.2.12}$$

$$\dot{M}_y = \gamma \left[-M_x B_0 + M_z B_1 \cos(\omega t) \right] - \frac{M_y}{T_2} \tag{1.2.13}$$

$$\dot{M}_z = -\gamma \left[M_x B_1 \cos(\omega t) + M_y B_1 \sin(\omega t) \right] - \frac{M_z - M_0}{T_1} \,. \tag{1.2.14}$$

1.3 Experimental Methods

To measure the characteristic times T_2^*, T_2, T_1 the probe is placed inside a magnetic field $\vec{B}_0$ created by large magnets and inside a coil which is used to apply the pulses and to measure the signal of the magnetic moments via induction.

1.3.1 Measurement of T_2^* via Free Induction Decay

To measure T_2^* a $\frac{\pi}{2}$-pulse is applied and the magnetization is flipped into the xy-plane. There it will decay due to the inhomogeneties of the magnetic field and the thereby induced dephasing. This method is called FREE INDUCTION DECAY. The determined T_2^* can then be used to approximate the inhomogeneity of the magnetic field.

1.3.2 Measurement of T_1 via Inversion Recovery

To measure the spin-lattice-relaxation a methode called INVERSION RECOVERY is used. First, the net magnetic moment is excited from the thermal equilibrium by flipping it. This is done by applying a π-pulse. The magnetization will now decay according to (1.2.8). After a certain time τ, a $\frac{\pi}{2}$-pulse is applied to bring the magnetization into the xy-plane where it can be detected and will decay according to (1.2.7). Measuring the initial amplitude of this decay in dependence of τ, the relaxation time T_1 can be determined.

1.3.3 Measurement of T_2

If the applied magnetic field would be perfectly homogeneous, no dephasing would occur and T_2 could be measured by FREE INDUCTION DECAY. However, due to dephasing this is not possible and more spohisticated methods must be applied. This is done by applying a series of $\frac{\pi}{2}$- and π-pulses. In general, applying a $\frac{\pi}{2}$-pulse, waiting a time τ and then applying a $\frac{\pi}{2}$-pulse inverts the magnetization and the dephasing. After a time 2τ the magnetizations are then again in phase which leads to a maximum in the detected signal called spin echo. By varying τ the FREE INDUCTION DECAY can be measured without dephasing effects. However, diffusion will take place inside the probe thus altering the net magnetization M_0 in each run of the experiment slightly, which will cause errors in the time T_2 determined by this method. The diffusion varies the distance between the spins or dipoles respectively. Thus the coupling between two dipoles or spins is affected. For strong diffusion and thus quickly changing distances the spins only interact for a short time. Therefore, the spin-spin relaxation time T_2 increases. Furthermore, between each measurement one has to wait at least a few times T_1 to saturates magnetization.

Carr-Purcell-Methode

Carr and Purcell introduced a method at which the applied a series of π-pulses in one single experiment and thus measuring several spin echos without measurable diffusion processes. The sequence they used reads $\frac{\pi}{2}, \tau, \pi, 2\tau, \pi, 2\tau, \ldots$. In addition to the saving of time, this method also reduces the error due to diffusion by a power of n^2 with respect to the Spin-Echo-Methode, where n is the number of data points taken. [3]

However, the pulse length of the applied pulses must be determined experimentally and furthermore the magnetic field can not be switched perfectly. This leads to errors due to rising and falling times. Thus, the error accumulates and increases with the length of the series.

Meiboom-Gill-Methode

Meiboom and Gill introduced an improvement of the Carr-Purcell-Methode to reduce the error caused by non-perfect pulse shapes and lengths. They exploited the fact, that applying and $(\pi + \delta)$-pulse clockwise and then anticlockwise i.e. a $-(\pi + \delta)$-pulse causes the error δ to vanish. Thus, every second echo is not biased by this error. Instead, the measurement is limited by the error of the error, which is orders of magnitudes smaller. The used pulse sequence of the Carr-Purcell-Methode reads $\frac{\pi}{2}, \tau, \pi + \delta, 2\tau, -(\pi + \delta), 2\tau, \pi + \delta, 2\tau, -(\pi + \delta) \ldots$

2 Experimental Setup and Procedure

2.1 Experimental Setup

A Techspin PS2-A spectrometer capable for both pulsed and CW NMR was used. It consists of two units, a permanent magnet with the pickup coil and the supply/receiver unit. A sketch of the setup can be found in fig. 2.1. The permanent magnet creates a homogenous field of approximated 0.5 T. The homogeneity of the field can be fine tuned by applying four field gradients, which can be set by a control unit. The pickup coil is connected to a capacitor and the receiver module. The eigenfrequency of this LC circuit can be tuned via fine-tuning of the capacitor.
The supply/receiver-unit consists of the receiver module with fixed gain low noise amplifier, a radio frequency synthesizer and a pulse programmer. It also contains a lock-in sweep module which is only required for cw-NMR. Further technical details of the components and the circuit diagrams can be found in [4].
The output signal was recored and analyzed with an oscilloscope.

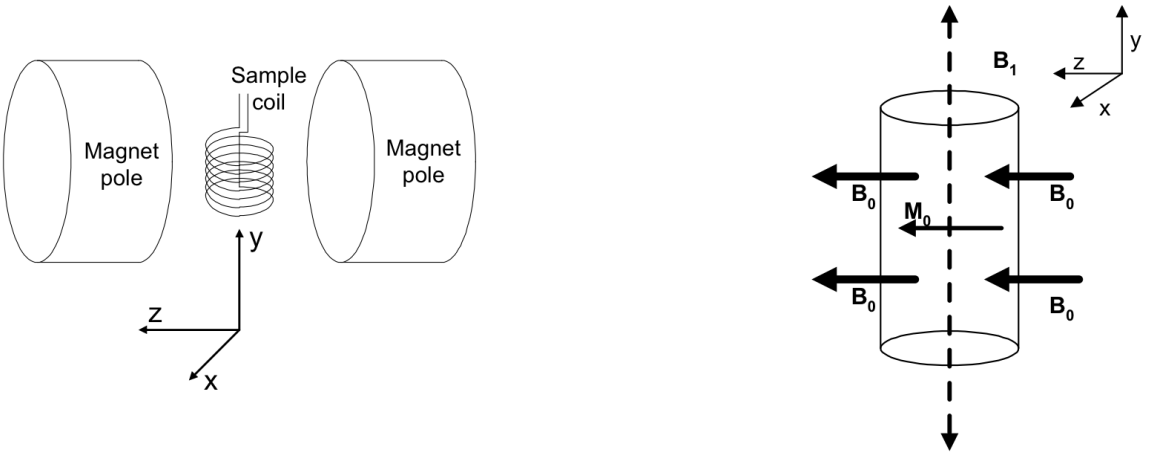

Fig. 2.1: Sketch of the basic system of experimental setup (*left*) and of the acting vector fields (*right*). [7].

2.2 Experimental Procedure

First the frequency synthesizer was tuned to the Larmor frequency by maximizing the FID signal at a pulse duration of approx. 7.5 μs and using the 0.2 mol solution of $CuSO_4$. The eigenfrequency of the LC circuit was tuned to be resonant with the Larmor frequency by placing a probe coil inside the pickup coil and maximizing the induced voltage in the probe coil

which was measured with the oscilloscope. These two tuning steps were performed iterative because a change of either of these two parameters affected the other one. The FID signal was maximal for a radio frequency of 21.000 MHz and the obtained peak-to-peak voltage was 56 V. Secondly, the pulse durations were calibrated which is documented in more detail in 3.1. Third, the inhomogeniety of the electric field was minimized by tuning the field gradients and thus maximizing the transversal relaxation time due to dephasing T_2^*. The relaxation times were measured with the different methods as described in 1.3. The position of the sample did not vary during the different measurements as a sample was placed inside the spectrometer and was changed only after all measurements were performed.

3 Experimental Results and Analysis

3.1 Calibration of Pulse Duration

The 0.2 mol solution of $CuSO_4$ was used to calibrate the pulse durations. The $\frac{\pi}{2}$-pulse was calibrated by maximizing the FID signal amplitude. In the interval of 2.88 μs up to 3.14 μs a constant and maximal amplitude of (2.00 ± 0.02) V was measured. By taking the mean value of this interval as pulse duration a value of $\tau_{\pi/2} = (3.03 \pm 0.13)\,\mu$s is obtained. Due to the fact that any odd multiple of $\frac{\pi}{2}$ can be used, also longer pulse durations corresponding to $\frac{3\pi}{2}$ and $\frac{5\pi}{2}$-pulses were examined. Considering the fact that a longer pulse duration minimizes the error caused by switching processes of the pulse, longer pulses seem more convenient. However, if the pulse duration is too long, errors due to diffusion have a larger impact. For a pulse duration of $\tau_{3\pi/2} = (9.7 \pm 0.1)\,\mu$s a larger amplitude of $(2,15 \pm 0.02)$ V is measured while for larger pulse the amplitude decreases. Thus, the $\frac{3\pi}{2}$-pulse was used instead of the $\frac{\pi}{2}$-pulse for most measurements. The π-pulse duration was calibrated by minimizing the FID-signal of an $(\pi, 0.3\,\mu\text{s}, \frac{\pi}{2})$ pulse series. Then, the pulse duration was fine tuned by minimizing the difference between the Carr-Purcell and Meiboom-Gill method and thus minimizing the angel error δ. A pulse duration of $\tau_\pi = (6.44 \pm 0.3)\,\mu$s was obtained by this method. For the $(\pi, 0.3\,\mu\text{s}, \frac{\pi}{2})$ pulse series a difference between Carr-Purcell and Meiboom-Gill was measurable while for the $(\pi, 0.3\,\mu\text{s}, \frac{3\pi}{2})$ pulse series no difference could be detected. This justifies the assumption, that a longer but not too long pulse is more suitable.

3.2 Inhomogeneity of the External Magnetic Field

Due to the fact, that the dephasing of the magnetic momenta is caused by the inhomogeneities of the external magnetic field $\vec{B}_0$, the inhomogeneity can be determined by measuring T_2^*. This was done by measuring a FID-signal for two different samples. By applying different magnetic field gradients the magnetic field could be tuned to minimize the inhomogeneity. According to (1.2.10) the decay time of the FID-signal is given by the relaxation time T_2^* and thus depends on the Larmor-frequency distribution which is proportional to the inhomogeneity of the field. The set values with yield the largest decay time T_2^* and therefore the minimal inhomogeneity are stated in tab. 3.1

X	Y	Z	Z^2
0	+8.45	+1.15	−5.36

Tab. 3.1: Readings of potentiometers for applied field gradients.

According to [8] the FID-signal is given by the Fourier transform of the magnetic field distribution. Thus, for a Gaussian field distribution function we expect

$$U_{\mathrm{FID}}(t) = U_0 \exp\left[-\left(\frac{t-t_0}{T_2^*}\right)^2\right] \tag{3.2.1}$$

while for an Lorentz field distribution function the expectation is

$$U'_{\mathrm{FID}}(t) = U_0 \exp\left[-\frac{t}{T_2^*}\right] . \tag{3.2.2}$$

The FID signal was measured for two different samples and the obtained data was fitted using MATHEMATICA's `NonlinearModelFit` with the model functions $U(t) = U_0 \exp[-t/T_2^*] + b$ for the Lorentzian and $U(t) = U_0 \exp\left[-(t - t_0/T_2^*)^2\right] + b$ for the Gaussian fit. The FWHM inhomogeneity can be calculated via

$$\Delta B_{gauss} = \frac{4\sqrt{\ln(2)}}{\gamma T_2^*} , \qquad \Delta B_{lorentz} = \frac{2}{\gamma T_2^*} . \tag{3.2.3}$$

The obtained parameters and plots are given in tab. 3.2, fig. 3.1 and fig. 3.2 respectively. The given error margin is determined by the standard error of the numerical fit. The calculation of inhomogeneity according to (3.2.3) is given in tab. 3.3, where the gyromagnetic ratio of a free proton $\gamma = 2.68 \cdot 10^8 s^{-1} T^{-1}$ [1] was used. From this data one can conclude, that the inhomogeneity of the field is approx. $6\,\mu$T or $\Delta B/B \approx 10^{-5}$.

Fit	Sample:	0.1 mol	0.2 mol
Lorentzian	U_0 [V]	2.21 ± 0.03	3.00 ± 0.03
	T_2^* [ms]	2.3 ± 0.1	1.34 ± 0.03
	b [V]	-0.24 ± 0.04	-0.07 ± 0.02
Gaussian	U_0 [V]	2.3 ± 0.1	4.6 ± 0.4
	T_2^* [ms]	2.29 ± 0.09	2.5 ± 0.2
	t_0 [ms]	-1.5 ± 0.1	-0.002 ± 0.001
	b [V]	0.09 ± 0.01	0.11 ± 0.01

Tab. 3.2: Parameters obtained by numerical fit of FID-signal

Sample	ΔB_{gauss} [μT]	$\Delta B_{lorentz}$ [μT]
0.1 mol	5.0 ± 0.5	3.3 ± 0.2
0.2 mol	5.4 ± 0.3	5.6 ± 0.2

Tab. 3.3: FWHM field inhomogeneities for different samples and fit models.

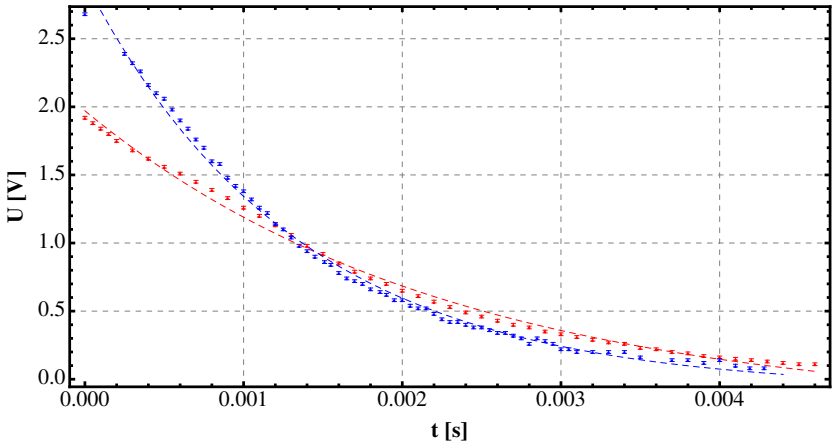

Fig. 3.1: Free Induction Decay signal. Induced voltage U in dependence on time t for different concentrations of $CuSO_4$ in water (red 0.1 mol and blue 0.2 mol). The dashed lines are obtained by numerical fits for a Lorentzian distribution function .

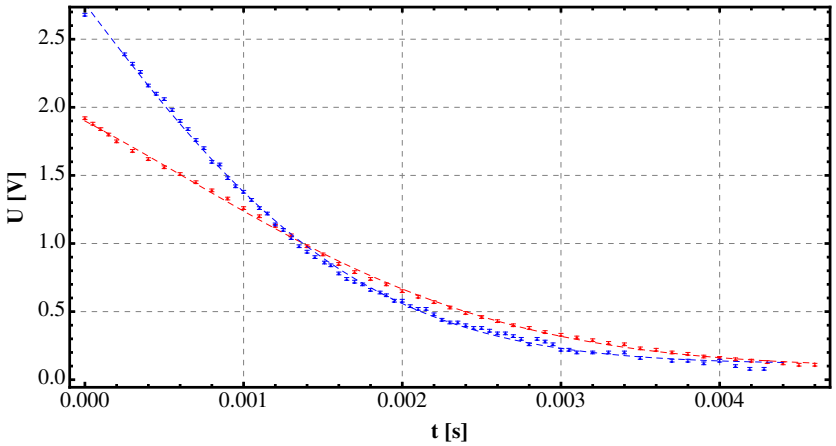

Fig. 3.2: Free Induction Decay signal. Induced voltage U in dependence on time t for different concentrations of $CuSO_4$ in water (red 0.1 mol and blue 0.2 mol). The dashed lines are obtained by numerical fits for a Gaussian distribution function.

3.3 Longitudinal Relaxation Time T_1

The longitudinal relaxation time was measured using a $(\pi, \tau, \frac{\pi}{2})$ or $(\pi, \tau, \frac{3\pi}{2})$ pulse sequence as described in 1.3.2. Solving the ordinary differential equation (1.2.8) yield

$$M_z(\tau) = M_0 \left(1 - 2e^{-\frac{\tau}{T_1}}\right) \tag{3.3.1}$$

where M_0 is the initial amplitude. To gain statistically more significant values, the build in averaging option of the oscilloscope was used to average over 32 samples. The obtained data was fitted using MATHEMATICA's `NonlinearModelFit` with the model function $V(\tau) = V_0 \operatorname{abs}[1 - 2\exp(-t/T_1)]$. The results are summarized in tab. 3.4 and fig. 3.3. The given error margin is determined by the standard error of the numerical fit due to the fact, that it is significantly larger then the read-off-errors of the oscilloscope. Any error caused by the inaccuracy of the pulse duration and therefore the angle at which the magnetization is tilted, does only affect M_0 due to projection. This shift however is constant for any value of τ. Therefore T_1 is not affected by this error. The data denoted with a asterix was obtained by using a $\frac{\pi}{2}$-pulse

Sample	V_0 [V]	T_1 [ms]
0.05 mol	1.87 ± 0.01	20.7 ± 0.2
0.1 mol	1.88 ± 0.01	10.3 ± 0.1
0.2 mol	2.67 ± 0.02	4.5 ± 0.1
0.2 mol*	2.69 ± 0.03	4.4 ± 0.1

Tab. 3.4: Parameters obtained by numerical fit of Inversion Recovery Measurement

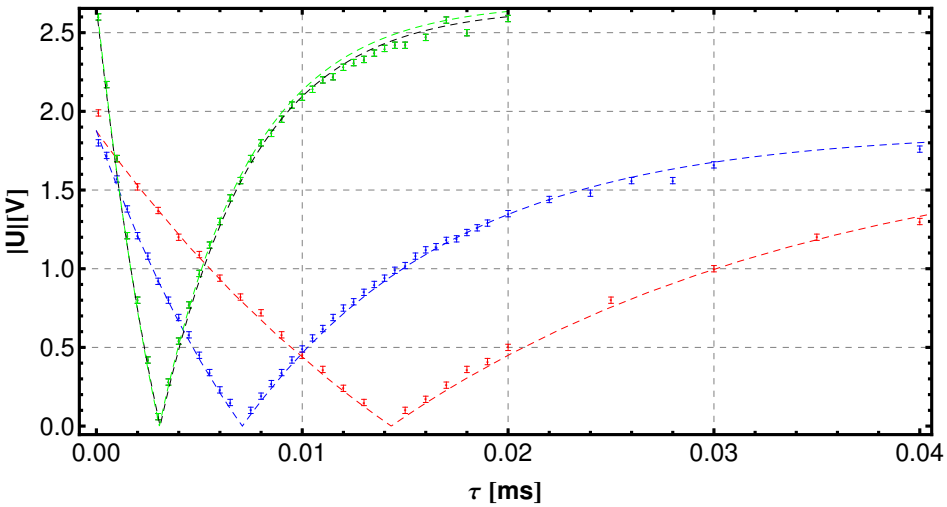

Fig. 3.3: Inversion Recovery amplitude in dependence on τ for different concentrations of $CuSO_4$ in water (red 0.05 mol, blue 0.1 mol, black 0.2 mol and green 0.2 mol obtained with a $\frac{\pi}{2}$-pulse). The dashed lines are obtained by numerical fits.

instead of an $\frac{3}{2}\pi$-pulse. However, both sets of data are identical within errors and the numerical

fit of both sets yield identical parameters. Thus, although longer pulse durations are used no significantly larger errors due to diffusion are detectable.

3.4 Transversal Relaxation Time T_2

3.4.1 Measurement via Spin-Echo-Methode

The transversal relaxation time was measured using a $(\frac{3}{2}\pi, \tau, \pi)$ pulse sequence as described in 1.3.3. The time elapsed between the initial signal and the spin echo signal amounts to 2τ and therefore the amplitude of the spin echo signal is given by

$$M_{xy}(\tau) = M_{xy,0}\, e^{-\frac{2\tau}{T_2}} \tag{3.4.1}$$

where $M_{xy,0}$ is the initial amplitude. To gain statistically more significant values, the build in averaging option of the oscilloscope was used to average over 32 samples. The obtained data was fitted using MATHEMATICA's `NonlinearModelFit` with the model function $V(\tau) = V_0 \exp[-2\tau/T_2] + c$. The results are summarized in tab. 3.5 and fig. 3.4. The given error margin is determined by the standard error of the numerical fit due to the fact, that it is significantly larger then the read-off-errors of the oscilloscope. Any error caused by the inaccuracy of the pulse duration and therefore the angle at which the magnetization is tilted, does only affect $M_{xy,0}$ due to projection. This shift however is constant for any value of τ. Therefore T_2 is not affected by this error.

Sample	V_0 [V]	T_2 [ms]	c [V]
0.05 mol	2.12 ± 0.03	19.0 ± 0.7	-0.15 ± 0.03
0.1 mol	1.92 ± 0.01	10.0 ± 0.1	-0.02 ± 0.01
0.2 mol	2.74 ± 0.02	4.1 ± 0.1	0.06 ± 0.01

Tab. 3.5: Parameters obtained by numerical fit of Spin Echo Measurement

3.4.2 Measurement via Carr-Purcell-Methode

The transversal relaxation time was measured using a $(\frac{3}{2}\pi, \tau, \pi, 2\tau, \pi, \ldots)$ pulse sequence as described in 1.3.3. A pulse-spacing of $\tau = 0.5 - 0.7$ ms depending on the concentration of $CuSO_4$ was used and $N = 35$ pulses were applied. The period was set to $P = 700$ms to allow the magnetization to regain the saturation value M_0 before a new measurement was started. The sign of the Z^2-gradient was inverted to reduce the width of the peaks and therefore allowed a more precise determination of peak value and position. This however did not affect the height of the peaks. To gain statistically more significant values, the build in averaging option of the oscilloscope was used to average over 32 samples. The obtained data was fitted using MATHEMATICA's `NonlinearModelFit` with the model function

$$V(\tau) = V_0 \exp[-t/T_2] + c\,. \tag{3.4.2}$$

As already mentioned, an error in the π-pulse duration and thus in the tilted angle will accumulate over time distorting the signal. To account for this error a cos-term was added to

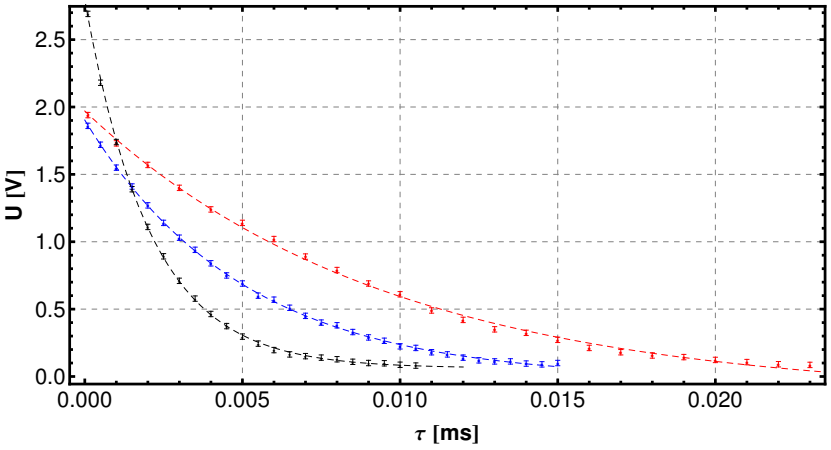

Fig. 3.4: Echo-signal amplitude in dependence on τ for different concentrations of $CuSO_4$ in water (red 0.05 mol, blue 0.1 mol and black 0.2 mol). The dashed lines are obtained by numerical fits.

the model function, which describes the projection of the magnetization onto the xy-plane. This model function reads

$$V'(\tau) = V_0' \exp\left[-\frac{t}{T_2'}\right] \cos\left(\frac{\delta t}{2\tau}\right) + c' \,. \tag{3.4.3}$$

The results are summarized in tab. 3.6, fig. 3.6 and tab. 3.7, fig. 3.5 respectivetly. The given error margin is determined by the standard error of the numerical fit due to the fact, that it is larger then the read-off-errors of the oscilloscope. From this data it is obvious, that the beat seen in the plots is not due to *cos*-type oscillation due to errors in the pulse durations for the samples with 0.05mol and 0.1mol respectively.

Sample	V_0' [V]	T_2' [ms]	c' [V]	$\delta[^\circ]$
0.05 mol	1.7 ± 0.1	10.1 ± 0.7	0.16 ± 0.05	$10^{-8} \pm 10^{7}$
0.1 mol	1.7 ± 0.1	5.1 ± 0.3	0.18 ± 0.02	$10^{-9} \pm 10^{9}$
0.2 mol	2.1 ± 0.1	4.3 ± 0.3	0.43 ± 0.07	12 ± 1
0.2 mol*	1.9 ± 0.1	5.2 ± 0.7	0.7 ± 0.1	18 ± 2

Tab. 3.6: Parameters obtained by numerical fit of Carr-Purcell Measurement using model function (3.4.3).

The data denoted with a asterix was obtained by using a $\frac{\pi}{2}$-pulse instead of and $\frac{3}{2}\pi$-pulse. Both sets of data differ slightly . This however, confirms our assumption, that the $\frac{3\pi}{2}$-pulse is better suited for this concentration, as the standard-deviations are significantly smaller.
The difference between the fits with and without the added cos-term yields that the better results can not be decided conclusively. For small concentrations both fits yield the same parameter and the error angle δ is numerically zero. Also, the large standard deviations are an indicator, that the numerical fits for smaller concentrations do not yield numerically sensible

Sample	V_0 [V]	T_2 [ms]	c [V]
0.05 mol	1.74 ± 0.04	10.1 ± 0.5	0.16 ± 0.02
0.1 mol	1.73 ± 0.02	5.1 ± 0.2	0.18 ± 0.02
0.2 mol	2.7 ± 0.08	3.7 ± 0.4	-0.00 ± 0.01
0.2 mol*	3.4 ± 0.4	5 ± 1	-0.8 ± 0.5

Tab. 3.7: Parameters obtained by numerical fit of Carr-Purcell Measurement using model function (3.4.2).

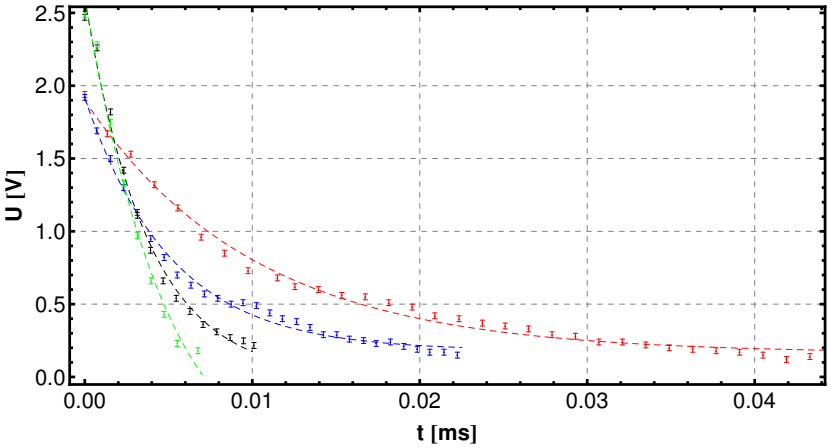

Fig. 3.5: Carr-Purcell-Signal for different concentrations of $CuSO_4$ in water (red 0.05 mol, blue 0.1 mol, black 0.2 mol and green 0.2 mol with a $\frac{\pi}{2}$-pulse). The dashed lines are obtained by numerical fits using model function (3.4.2).

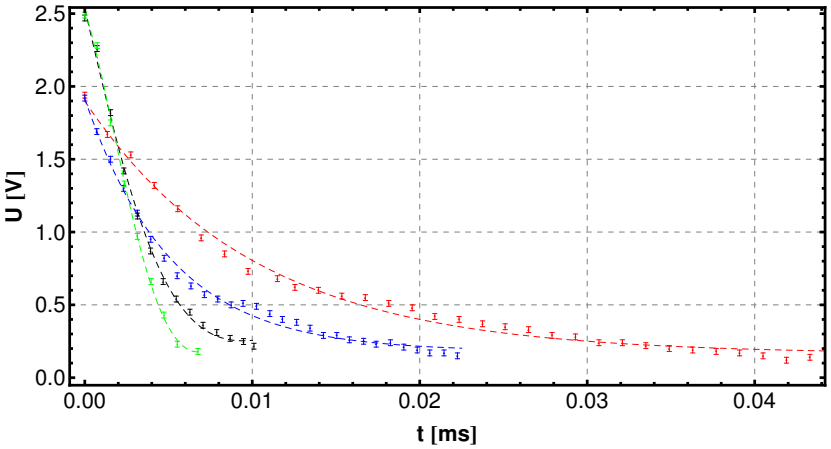

Fig. 3.6: Carr-Purcell-Signal for different concentrations of $CuSO_4$ in water (red 0.05 mol, blue 0.1 mol, black 0.2 mol and green 0.2 mol with a $\frac{\pi}{2}$-pulse). The dashed lines are obtained by numerical fits using model function (3.4.3).

parameters for the angle δ. However, for larger concentrations the fits with the added cos-term fit the data better (cf. fig. 3.7 and fig. 3.8).

3.4.3 Measurement via Meiboom-Gill-Methode

The transversal relaxation time was measured using a $(\frac{3}{2}\pi, \tau, \pi, 2\tau, -\pi, \ldots)$ pulse sequence as described in 1.3.3. A pulse-spacing of $\tau = 0.5 - 0.7\,\text{ms}$ depending on the concentration of $CuSO_4$ was used and $N = 35$ pulses were applied. The period was set to $P = 700\text{ms}$ to allow the magnetization to regain the saturation value M_0 before a new measurement was started. The sign of the Z^2-gradient was inverted to reduce the width of the peaks and therefore allowed a more precise determination of peak value and position. This however did not affect the hight of the peaks. To gain statistically more significant values, the build in averaging option of the oscilloscope was used to average over 32 samples. The obtained data was fitted using MATHEMATICA's `NonlinearModelFit` with the model function

$$V(\tau) = V_0 \exp\left[-t/T_2\right] + c\,. \tag{3.4.4}$$

The fit was done first regarding only odd indices and second only regarding even indices. The results are summarized in tab. 3.8, fig. 3.7 and fig. 3.8. The given error margin is determined by the standard error of the numerical fit due to the fact, that it is significantly larger then the read-off-errors of the oscilloscope. The fits were performed first using only odd and therefore defective data points and a second time only regarding the even, non-defective data points.
The data denoted with a asterix was obtained by using a $\frac{\pi}{2}$-pulse instead of and $\frac{3}{2}\pi$-pulse. Both sets of data differ from each other. The fits of the data obtained with $\frac{3\pi}{2}$-pulse yield again slightly better values with respect to standard deviations of the fitted parameters.

Sample	V_0 [V]	T_2 [ms]	c [V]	V_0 [V]	T_2 [ms]	c [V]
0.05 mol	1.8 ± 0.03	13.8 ± 0.6	0.10 ± 0.02	1.76 ± 0.04	13.6 ± 0.8	0.12 ± 0.03
0.1 mol	1.74 ± 0.02	6.4 ± 0.3	0.16 ± 0.03	1.68 ± 0.05	6.8 ± 0.9	0.14 ± 0.03
0.2 mol	2.54 ± 0.08	4.1 ± 0.4	0.00 ± 0.01	2.71 ± 0.02	3.5 ± 0.1	0.09 ± 0.02
0.2 mol*	2.60 ± 0.07	5.0 ± 0.4	-0.08 ± 0.07	2.71 ± 0.03	4.0 ± 0.2	0.04 ± 0.03

Tab. 3.8: Parameters obtained by numerical fit of Meiboom-Gill Measurement. On the left hand side are the fits using the odd indices and on the right hand side the even indices.

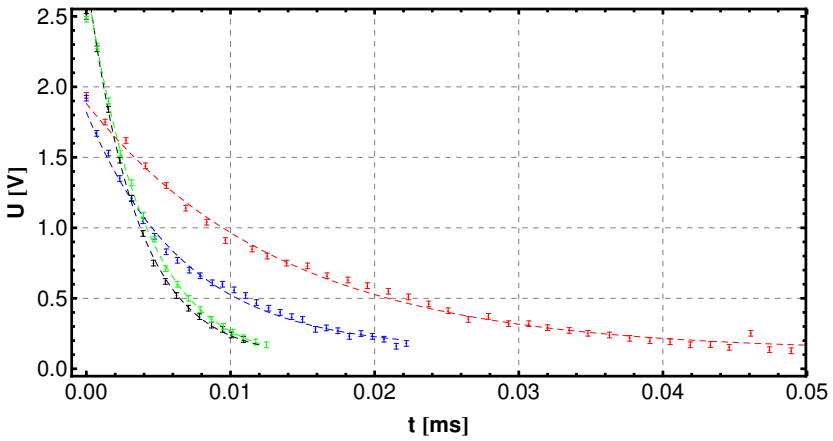

Fig. 3.7: Meiboom-Gill-Signal for different concentrations of $CuSO_4$ in water (red 0.05 mol, blue 0.1 mol, black 0.2 mol and green 0.2 mol with a $\frac{\pi}{2}$-pulse). The dashed lines are obtained by numerical fits using only even indices.

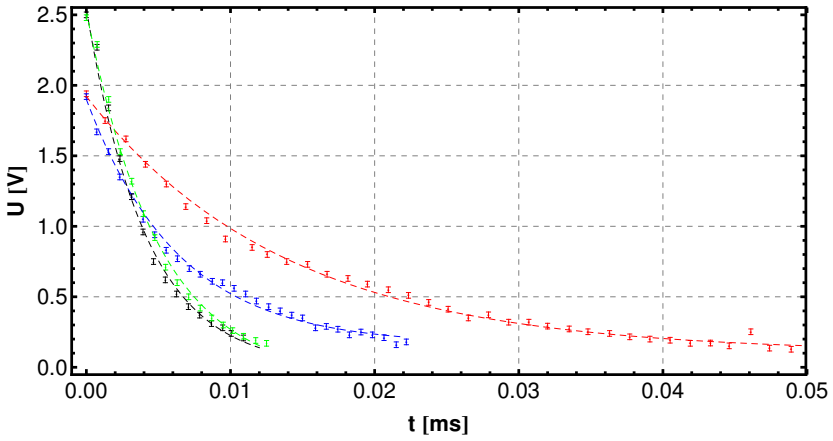

Fig. 3.8: Meiboom-Gill-Signal for different concentrations of $CuSO_4$ in water (red 0.05 mol, blue 0.1 mol, black 0.2 mol and green 0.2 mol with a $\frac{\pi}{2}$-pulse). The dashed lines are obtained by numerical fits using only odd indices.

3.5 Influence of Concentration of $CuSO_4$

According to (1.2.11) we expect an anti-proportional relation between the concentration of $CuSO_4$ and the several relaxation times. In fig. 3.9 the relaxation times are plotted over the inverse concentration and tab. 3.9 shows the parameters obtained by linear regression. However, with only three data points per data set a linear regression is not very conclusive.

Methode	$1/\alpha$ [ms mol^{-1}]	c [ms]
Inversion Recovery	1.08 ± 0.02	-0.9 ± 0.2
Spin Echo	0.98 ± 0.07	-0.4 ± 0.9
Carr-Purcell	0.43 ± 0.06	1.2 ± 0.7
Meiboom-Gill	0.68 ± 0.01	0.05 ± 0.03

Tab. 3.9: Parameters obtained by linear regression of relaxation times in dependence on concentration of $CuSO_4$

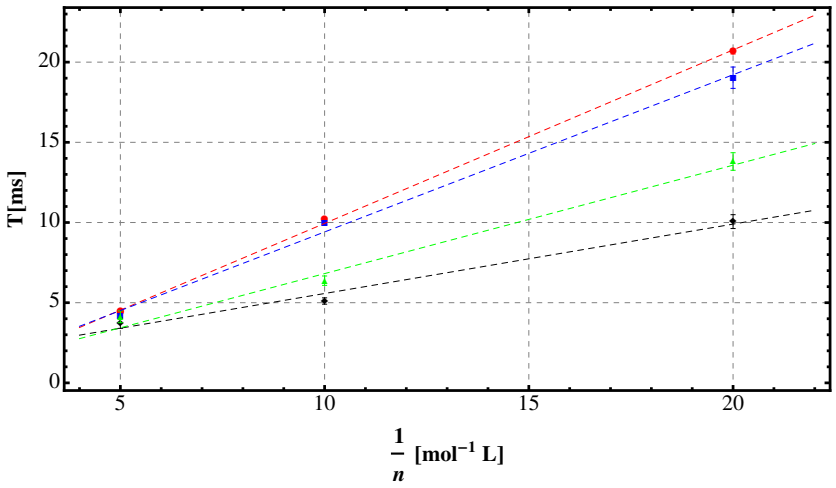

Fig. 3.9: Relaxation times in dependence on concentrations of $CuSO_4$ in water. The dashed lines are obtained by numerical fits. (Green: Meiboom-Gill; Black: Carr-Purcell; Blue: Spin Echo; Red: Inversion Recovery.)

4 Conclusion

By maximizing the FID signal it was possible to tune the frequency of the emitted magnetic pulse to the Lamor frequency of the protons and to set the eigenfrequency of the detecting LC-circuit by maximizing the induced voltage. The pulse durations of different pulses were also determined for $\frac{\pi}{2}$-, $\frac{3\pi}{2}$- and π-pulses by maximizing the FID signal or minimizing the Spin-echo signal respectively. The pulse durations were fine tuned by comparing the signal of the Carr-Purcell-Methode and the Meiboom-Gill-Methode.

The inhomogeneity of the external magnetic field could be tuned by applying adjustable magnetic gradients. The resulting inhomogeneity could be measured by measuring T_2^* via Free Induction Decay with two samples of different concentration of paramagnetic $CuSO_4$. The obtained data was fitted both with a Lorentzian and a Gaussian distribution function of the magnetic field. Both fits yielded similar values. However, the Gaussian model function fitted the obtained data better, which can be seen by comparing fig. 3.2 with fig. 3.1. The determined inhomogeneity of the magnetic field was $\Delta B = 6\,\mu\mathrm{T}$ or $\Delta B/B = 10^{-3}\,\%$.

The longitudinal relaxation times of spin protons in water with different concentrations of paramagnetic $CuSO_4$ were investigated via Inversion Recovery. The results are summarized in tab. 4.1. As expect, a linear dependence of the relaxation time on the inverse concentration was found. To evaluate the method, the value for 0.1 mol $CuSO_4$ concentration are compared with literature values. Pope et al. [9] used different methods and found T_1 in the range of 12.0 ± 0.6 to $15.2 \pm 0.2\,\mathrm{ms}$. This value is compatible with our result.

The transversal relaxation times of spin protons in water with different concentrations of paramagnetic $CuSO_4$ were investigated via different methods. The results are summarized in tab. 4.1. The results of all measurements for smaller concentrations are compatible with each other i.e. the threefold error margins overlap with the exception of Spin Echo. Due to the fact, that errors caused by dephasing or poorly determined pulse durations only decreases the relaxation times, it is valid to assume, that the methods which yields larger relaxation times are more reliable. In consequence, the spin echo method yield the more reliable relaxations times while the Carr-Purcell-Method is off by a factor ≈ 2 for all concentrations except 0.2 mol. The Meiboom-Gill-Methode provides values that are better than the ones obtained by Carr-Purcell but still significantly smaller than the values obtained by Spin-Echo.
The Meiboom-Gill-Methode provides only reliable values for larger concentrations of $CuSO_4$. Reexamining the data yields, that the numerical fits matches the recorded data. Regarding an possible error in the pulse duration during the Carr-Purcell-measurements by adding and cos-term does not significantly improve the fits. Additionally, the fits of Carr-Purcell-data and Meiboom-Gill-data do not deviate strongly from each other. Also, the fits of the Meiboom-Gill-data regarding only odd and thus defective data is equal to the fits of the even data points. Thus, an error in pulse duration and angle can be excluded.

Sample	T_1 [ms]	$T_{2,\mathrm{SE}}$ [ms]	$T'_{2,\mathrm{CP}}$ [ms]	$T_{2,\mathrm{CP}}$ [ms]	$T_{2,\mathrm{MG}}$ [ms]
0.05 mol	20.7 ± 0.2	19.0 ± 0.7	10.1 ± 0.7	10.1 ± 0.5	13.6 ± 0.8
0.1 mol	10.3 ± 0.1	10.0 ± 0.1	5.1 ± 0.3	5.1 ± 0.2	6.8 ± 0.9
0.2 mol	4.5 ± 0.1	4.1 ± 0.1	4.3 ± 0.3	3.7 ± 0.4	3.5 ± 0.1
0.2 mol*	4.4 ± 0.1	N/A	5.2 ± 0.7	5 ± 1	4.0 ± 0.2

Tab. 4.1: Results for the different relaxation times obtained by different methods and concentration

For a concentration of 0.2 mol all measurements are compatible with each other. Especially the measurements for this sample with the different pulse durations ($\frac{\pi}{2}$- and $\frac{3\pi}{2}$-pulses) are equal within errors, but the measurements with the $\frac{\pi}{2}$-pulse have the larger errors. Furthermore, the system is invariant under rotation along the z-axis. Thus, a $\frac{\pi}{2}$-rotation into the xy-plane maps into a $\frac{3\pi}{2}$-rotation into the same plane. Furthermore, any relaxation takes place on a milisecond scale, while the scale at which rotation takes place is three order of magnitudes smaller (microseconds). Thus, the discrepancy between this measurements cannot by explained by the pulse duration per se. However, the control measurement to determine if any deviations exist between $\frac{3\pi}{2}$ and $\frac{\pi}{2}$ was taken for the sample of 0.2 mol concentration. For this sample, the $\frac{3\pi}{2}$-data-sets obtained by the Meiboom-Gill-Method and the Carr-Purcell-Method yield compatible values. However, for the other concentrations no measurements were done to invest if any deviations are present. Taking a closer look to the recorded data, a deviation between Spin-Echo measurements and Carr-Purcell or Meiboom-Gill respectively can be seen, as shown in fig. 4.1, for all concentrations except 0.2 mol. The cause of this deviation is unknown and not enough data was obtained for a thorough examination. These deviations are likely to be the reason for the strong discrepancy of the obtained values. That this deviations are caused by the longer pulse durations by causing noise or other unconsidered effects is the most probable assumption. To verify this, more data is needed particularly with regard to small concentrations and different pulse durations. If the longer pulses are the cause of this deviations, it is advisable to use shorter pulses instead.
It can be concluded, that the first impression, that the Spin-Echo-Method yields the better results, is reasonable. Furthermore, Pope et al. [9] found for T_2 a value between 12.0 ± 0.2 and 15.2 ± 0.2 ms. This values are not in the threefold error margins of any of our measurements. However, the value obtained by Spin-Echo deviates only by 17 %, confirming our thesis, that the Spin-Echo yields the more reasonable value.

The deviations also affected the analysis of the dependence of relaxations times on concentration of $CuSO_4$. All data sets show a linear dependence on n^{-1}. However, the expectation, that all relaxations times show in first non-vanishing order the same proportionality factor α cannot be confirmed. Nevertheless, comparing only the reliable measurements of the longitudinal relaxation time T_1 by Inversion Recovery and of the transversal relaxation time T_2 by Spin Echo, yield an factor $k = \alpha^{-1} = 1\,\mathrm{ms\,mol^{-1}}$. The other measurements are as before of by a factor ≈ 2 for the Carr-Purcell-measurment and slightly smaller for Meiboom-Gill. However, this is endowed with a high error margin, because only three points were available for each linear fit.

Pure water was also studied quantitatively. As expected, the decay times are several orders of magnitude larger than in all of the studied samples.

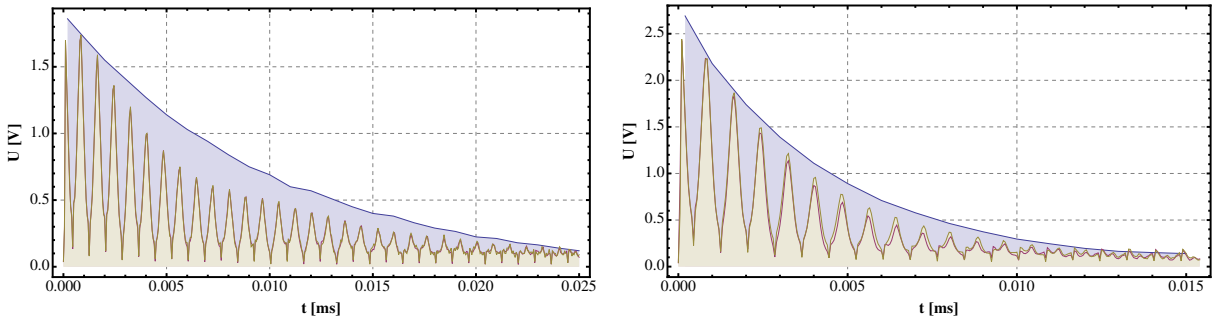

(a) 0.1 mol (b) 0.2 mol

Fig. 4.1: Plot of the different data as recorded by the oscilloscope for two different concentrations. The Spin-Echo signal is plotted in blue, the Meiboom-Gill and Carr-Purcell are plotted in beige. For (a) the signals show a strong deviation from the Spin-Echo signal which is not detectable in (b).

Bibliography

[1] Mohr, P. J.; Taylor, B. N.; Newell, D. B.; *CODATA recommended values of the fundamental physical constants: 2006*; Rev. Mod. Phys. 80, 2 pp 633 - 730; 2008

[2] Carrington, A.; McLachlan, A. D.; *Introduction to Magnetic Resonance*; Harper & Row; New York; 1969

[3] Cowan, B.; *Nuclear Magnetic Resonance and Relaxation*; Cambridge University Press; 1997

[4] Manual of the PS2-A spectrometer (TeachSpin)

[5] Slichter, C. P.; *Principles of Magnetic Resonance*; Springer; New York; 1969

[6] Farrar, T. C.; Becker, E. D.; *Pulse and Fourier Transform NMR*; Academic Press; New York: 1971

[7] Wolff-Reichert, B.; *Conceptual Tour of PNMR*; 2008

[8] *Ma 3 - Pulsed Nuclear Magnetic Resonance*; Instructions for the Advanced Laboratory Course at Freie Universität Berlin; 2011

[9] J.M. Pope; N. Repin; *A simple approach to T2 imaging in MRI*; Magnetic Resonance Imaging; Volume 6, Issue 6; 641-646; 1988